Plasmonic Photocatalysis with Metal-Semiconductor Hybrid Nanostructures

A thesis submitted to

Indian Institute of Science Education and Research Pune in partial fulfilment of the requirements for the BS-MS Dual Degree Programme

Indian Institute of Science Education and Research Pune

Dr. Homi Bhabha Road,

Pashan, Pune 411008, India

by

Namitha Deepak

(Reg No: 20191131)

Under the guidance of

Dr. Pramod P. Pillai

Certificate

This is to certify that this dissertation entitled **Plasmonic Photocatalysis with Metal-Semiconductor Hybrid Nanostructures** towards the partial fulfilment of the BS-MS dual degree programme at the Indian Institute of Science Education and Research, Pune represents study/work carried out by **Namitha Deepak** at the Indian Institute of Science Education and Research under the supervision of **Dr. Pramod P. Pillai**, Associate Professor, Department of Chemistry, during the academic year 2023-2024.

Signature of Student

Signature of Supervisor

Date : 27 March 2024

This thesis is dedicated to
Amma & Acha

Declaration

I hereby declare that the matter embodied in the report entitled **'Plasmonic Photocatalysis with Metal-Semiconductor Hybrid Nanostructures'** are the results of the work carried out by me at the Department of Chemistry, Indian Institute of Science Education and Research, Pune, under the supervision of Dr. Pramod P. Pillai and the same has not been submitted elsewhere for any other degree. Wherever others contribute, every effort is made to indicate this clearly, with due reference to the literature and acknowledgement of collaborative research and discussions.

Signature of Student

Signature of Supervisor

Date : 27 March 2024

Acknowledgement

This thesis attained this shape with the help of many individuals. I would like to thank each and everyone profusely for their contributions.

I am forever indebted to my supervisor, Dr. Pramod P. Pillai; thank you for introducing me to research and for the opportunities, constant input, helpful discussions, and suggestions given to me. I would like to wholeheartedly thank you for the guidance and support throughout the project.

I'm extremely grateful to my TAC member, *Dr. Angshuman Nag*, for the valuable discussions and the lessons. Thank you for giving me an opportunity to learn from you and for guiding me in my early days.

I would like to thank *Ms. Vanshika Jain* for all the lessons you taught me about science and life. Thank you for tolerating me and my poor jokes throughout. The effort you took in molding me, the constant support you provided, and the initiative to inculcate a love for research in me mean a lot as a student stepping into science. I've learned a great deal from you, and I consider myself extremely lucky to have been your mentee.

Nanoalchemy lab truly was like a second home to me; all the lab members: *Sumit, Indra, Pradyut, Kashyap, Vanshika, Ankit, Shreya, Adhra, Angela, Mridul* and *Sujitha*, who have regularly put in the effort to create a great environment for learning. Thank you for spending time to teach me various laboratory and life skills. The conversations over chai and the insights on the wild assortment of topics created memorable moments that I'll cherish forever.

I would like to acknowledge IISER Pune for the incredible set of students, faculty, staff, facilities, and infrastructure. I would like to acknowledge DST-Inspire for the financial support provided to me.

I am grateful for my friends, both near and far; I cannot fathom how life would have been without you people in my life, thank you for being my biggest and cheerleaders.

Finally, If I were to count my blessings, my family would be number one. I'm most thankful for my parents, who have been the pillars of support during everything, my grandmother, who taught me to dream, and my late grandfather, who gave me the courage to pursue my dreams; thank you for giving me a beautiful life filled with happiness and joy.

Table of Contents

List of Figures

List of Tables

Abstract

Photocatalysis with plasmonic nanoparticles (NPs) is emerging as an attractive strategy to make and break chemical bonds in a sustainable fashion. However, the fast relaxation dynamics of the photoexcited charge carriers in plasmonic NPs has often led to poor photocatalytic conversions. To overcome these limitations, the separation and extraction of photoexcited hot charge carriers must be faster than the thermalization process. This demands the integration of rationally chosen materials to construct hybrid plasmonic photocatalysts. Heterostructure containing plasmonic metal and semiconductor NPs is one such hybrid material that could suppress the recombination of photoexcited charge carriers, thereby improving the overall performance of plasmonic photocatalysis. In this work, the enhanced photocatalytic activity of gold nanoparticle – titanium dioxide metal-semiconductor heterostructure (Au-TiO_2) is used for the efficient regeneration of nicotinamide (NADH) cofactors under visible-light irradiation. The modification of plasmonic AuNPs with n-type TiO_2 semiconductor enhanced the charge separation process under visible-light excitation, because of the Schottky barrier formed at the Au-TiO_2 heterojunction. This led to a 12-fold increment in the photocatalytic activity of plasmonic AuNP in regenerating NADH cofactor. Detailed mechanistic studies revealed that the integration of TiO_2 semiconductor into plasmonic AuNPs led to the modification of the reaction pathway as well. Au-TiO_2 hybrid photocatalyst followed a less-explored light-independent pathway, in comparison to the conventional light-dependent path followed by the sole AuNP photocatalyst. The stark difference in the reaction mechanism with sole AuNP and Au-TiO_2 hybrid photocatalyst also profoundly impacted the reaction yield, where the NADH regeneration yield reached ~70 % in the light-independent pathway under optimized conditions. Furthermore, the change in reaction mechanism also alleviated the issues of product degradation under prolonged irradiation, as is commonly seen in photocatalytic NADH regeneration in literature. Thus, our study emphasizes the rational choice of components in hybrid nanostructures in dictating the photocatalytic activity and the underlying reaction mechanism in plasmon-powered chemical transformations.

Chapter 1 *Introduction*

Light-to-chemical energy conversion with nanoparticles is one of the widely explored areas in the scientific community. In this direction, photochemical transformations with plasmonic metal nanoparticles (NPs) under visible light irradiation resulted in a new avenue in photocatalysis- plasmonic photocatalysis [1-7] because of localized surface plasmon resonance (LSPR). LSPR is achieved when the frequency of the coherent oscillation of the electron cloud matches with the frequency of the incident light.[1-7] Because of the strong light-matter interaction at LSPR frequency, the visible-light absorption cross-section exceeds the geometric cross-section of metal NPs leading to an exceptionally high molar extinction coefficient (10^8-10^{10} M^{-1} cm^{-1}).[8] Such strong light absorption attributes result in a large charge carrier density in plasmonic NPs upon photoexcitation, allowing one to perform various chemical transformations under visible-light irradiation.[1-5] Plasmonic excitation generates highly energetic charge carriers, which undergoes a series of relaxation processes such as electron-electron, electron-phonon, and phonon-phonon scattering (Scheme 1.1).[8-11] The generated hot charge carriers can trigger various classes of chemical transformations, for instance, strong bond dissociation redox reactions, organic transformations, etc.[8-11] As can be seen from Scheme 1.1, the photoexcited charge carriers lose their energy within a small window of time ranging from fs to ps. This imposes several constraints on carrying plasmonic photocatalytic reactions in an efficient manner. Alongside this, the 'noble' surface of widely used plasmonic NPs limits the interaction with many of the substrates/reactants.[11,12] As a result, plasmonically photocatalyzed reactions proceed with low yields and selectivity.[11,12]

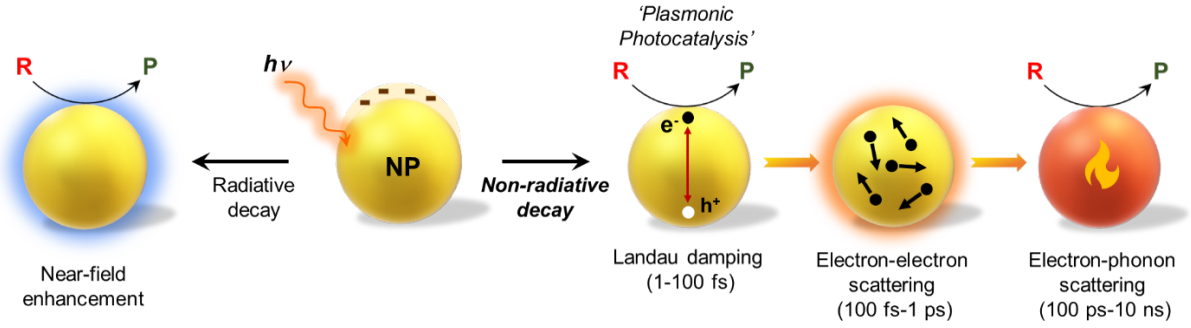

Scheme 1.1: Schematics representing the plasmon excitation and relaxation dynamics.

To circumvent these challenges, strategies must be developed for the faster extraction of charge carriers as well as the promotion of catalyst-reactant interactions. Inspired by the early works of Tatsuma and co-workers[13,14], the construction of hybrid nanostructures with metal NPs can facilitate the efficient charge separation from the plasmonic counterpart, as well as provide better substrate interaction with the catalyst surface. In this direction, continuous efforts are made to optimize different nanoparticle morphologies, configurations, and compositions to create a library of hybrid materials that can result in accelerated chemical transformations. In general, these hybrid nanostructures can broadly be classified into three categories: plasmonic metal-metal, plasmonic metal-semiconductor, and plasmonic metal-molecule heterostructures.[15,16] The choice of components in a heterostructure strongly depends on the electronic structure of the materials as well as the thermodynamics of the chosen reaction.[15,16]

In this work, we have focused on developing plasmonic metal-semiconductor-based hybrid nanostructures to carry out nicotinamide cofactor (NADH) regeneration under visible light irradiation. Nicotinamide cofactors are a key part of biocatalytic reactions driven by oxidoreductase enzymes, and their continuous regeneration is of much importance in devising artificial photosynthetic systems.[17,18] Previous works from our group have already revealed the power of *'sole'* plasmonic photocatalysis with gold nanoparticles (AuNPs) to regenerate NADH cofactor from NAD^+ in the presence of TEOA (triethanolamine) as the hole scavenger with visible light irradiation.[23] To accelerate the yield of the reaction, here, we have utilized Au and titanium dioxide (TiO_2) based metal-semiconductor hybrid nanostructures to facilitate better charge carrier separation resulting from the Schottky barrier formed at the interface (Scheme 1.2). Upon continuous irradiation with the visible light (corresponding to the LSPR frequency of the AuNPs), the hot charge carriers generated in Au, which attain energies greater than the Schottky barrier, are transferred to the conduction band (CB) of TiO_2 within tens to hundreds of femtoseconds.[27-30] Consequently, the electrons that accumulate in CB will participate in the reduction events, whereas the holes left in the Au core participate in the oxidation half-reactions. The efficiency of electron transfer from metal to semiconductor depends on the Schottky barrier values, Φ_{SB}.[27-30] A lower Φ_{SB} value often results in back-electron transfer to metal (charge recombination), whereas a higher Φ_{SB} value restricts electron transfer from metal to semiconductor.[27-

[30] In this regard, Au and TiO_2 form a heterojunction with appropriate Φ_{SB} ~ 1.1 eV with electron transfer efficiencies reaching ~45 %.[29,30]

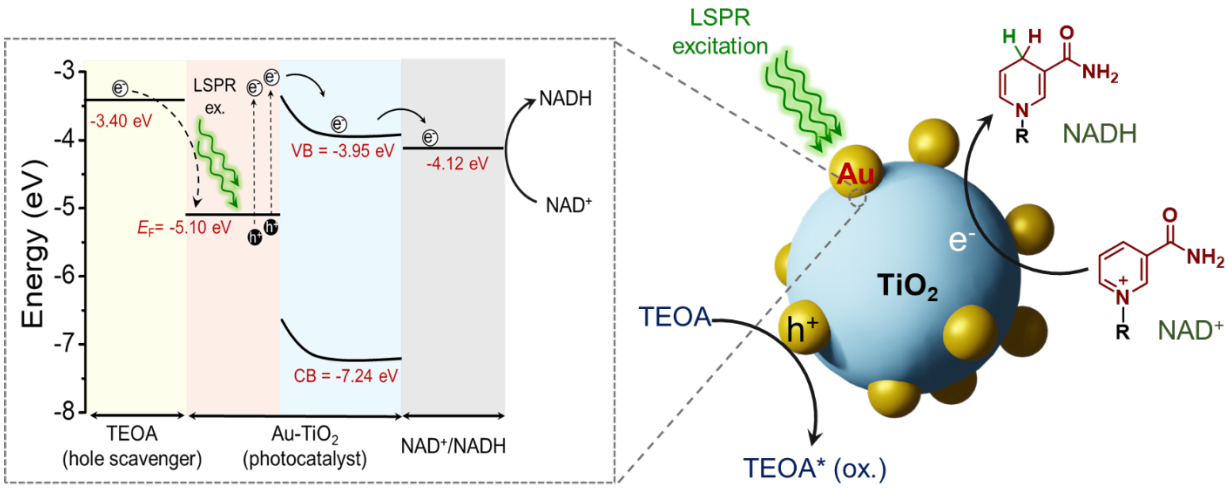

Scheme 1.2: Schematic illustration of the regeneration of NADH cofactor with Au-TiO_2 hybrid nanostructure under visible-light plasmonic excitation.

In our studies, the illumination of Au-TiO_2 hybrid photocatalyst with 532 nm light resulted in ~30 % NAD^+ conversion, which was ~12 folds higher than the sole AuNP based photocatalyst. Interestingly, NADH regeneration with Au-TiO_2 followed a mechanistically different path as compared to only AuNPs reported in prior literature. The reaction was found to proceed in two stages, where the oxidation product formed during the light reaction subsequently reduces the NAD^+ cofactor in the light-independent (dark) reaction to form NADH. Moreover, this change in reaction mechanism alleviated the issues related to the photodegradation of cofactors under prolonged irradiation. Under the optimized light-dark cascade reaction conditions, an excellent NAD+ conversion yield of ~70 % was achieved.

In short, not only does our study show the importance of hybrid nanostructures in enhancing plasmonic photocatalysis, but it also emphasizes the crucial role of the reactivity and nature of the components in the hybrid nanostructures, which can possibly result in unprecedented reaction mechanisms.

Chapter 2 Materials and Methods

2.1. Materials and Reagents:

Gold chloride trihydrate ($HAuCl_4.3H_2O$), titanium (IV) dioxide (TiO_2), sodium borohydride ($NaBH_4$), β-nicotinamide adenine dinucleotide sodium salt (NAD^+), β-nicotinamide adenine dinucleotide reduced disodium salt (NADH), sodium phosphate dibasic dihydrate ($Na_2HPO_4.2H_2O$), and sodium phosphate monobasic (NaH_2PO_4) were purchased from Sigma-Aldrich. Triethanolamine (TEOA) was purchased from Avra Chemicals. Glycolaldehyde dimer was purchased from BLD Pharmatech (India) Pvt Ltd. All the reagents were used as received without any further purification.

2.2. Synthesis of Au-TiO_2 Hybrid Nanostructure:

The desired Au-TiO_2 based hybrid plasmonic metal-semiconductor nanostructures were prepared following an in-situ borohydride reduction method by modifying the reported literature.[31] In a typical synthesis, 500 mg of commercially available TiO_2 nanoparticles (used as received) were dispersed in water, to which different amounts of 50 mM $HAuCl_4$ were added. To the resulting suspension, 1 mL of 0.1 M $NaBH_4$ was added under vigorous stirring conditions. An immediate color change from white to pink was observed, indicating the formation of Au NPs. The resultant suspension was stirred for 12 h to completely reduce $HAuCl_4$ and decompose excess $NaBH_4$. Thus, prepared Au-TiO_2 hybrid nanostructures were obtained by centrifugation, followed by drying under vacuum to obtain in a powdered form. The hybrid nanostructures with different Au content were labeled as AT-X (where X = 1 - 5).

2.3. Characterization Techniques:

2.3.1. Transmission Electron Microscopic (TEM) Studies:

TEM imaging was performed with JEOL JEM-2200FS HRTEM instrument. The photocatalyst samples were sonicated in water and drop-casted on a 400-mesh carbon-coated copper grid (Ted Pella Inc.). The excess solvent was removed, and the thus prepared grid was dried under vacuum before imaging.

2.3.2. Inductively Coupled Plasma Mass Spectroscopy (ICP-MS) Studies:

ICP-MS analysis for different Au-TiO_2 hybrid nanostructures was performed on Thermo Scientific iCAP Q ICP-MS instruments. For analysis, 5 mg of the photocatalyst sample was digested in H_2SO_4 at 270 ^oC, followed by adding aqua regia. All prepared samples were diluted with 0.32 N HNO_3, followed by filtration with a 0.22-micron syringe filter before analysis.

2.3.3. Photocurrent Measurements:

Photocurrent measurements were performed with Metrohm DropSens potentiostat using a three-electrode system with Au-TiO_2 coated FTO plate as the working electrode, Ag/AgCl as the reference electrode, and Pt wire as the counter electrode respectively. 1 cm^2 of the FTO plate was coated with different photocatalysts using a doctor blade method. The FTO was irradiated by 532 nm LEDs (~230 mW cm^{-2}) to collect the current response upon irradiation. Photocurrent measurements were carried out under chopped light conditions with 30s intervals between each cycle for at least 10 cycles for all the samples.

2.4. Photocatalytic Reduction of NAD^+ to NADH:

The photocatalytic experiments were carried out in a glass test tube under continuous irradiation with 2 x 10 W LEDs of 532 nm (light intensity falling on the test tube is ~ 230 mW cm^{-2} as measured with an optical power meter from Newport Model 842 PE). A typical reaction mixture consists of 5 mg of Au-TiO_2 (photocatalyst), 1 M TEOA (hole scavenger), and 1 mM NAD^+ in 50 mM phosphate buffer (pH 7.4). The pH of the final reaction mixture was adjusted to 8.[23] Subsequently, the reaction mixture was subjected to continuous visible-light irradiation for 10 h. The photocatalyst was removed by centrifuging the reaction mixture, and the photoregenerated NADH present in the supernatant was quantified using UV-visible absorption spectroscopy. The UV-vis absorption measurements were carried out with Shimadzu UV-3600 plus UV-vis-NIR spectrophotometer. The photoregenerated NADH yield was calculated by monitoring the absorbance at ~340 nm using the Beer-Lambert law as follow:[32]

$$C_{NADH} = \frac{A_{340}}{\varepsilon . l} \qquad (1)$$

Where, C is the concentration of regenerated NADH, A is the absorbance at 340 nm, ε is the molar extinction coefficient of NADH (6220 M^{-1} cm^{-1}), and *l* is the optical path length of 1 cm. The photoconversion yield was calculated using the following equation:

$$NADH\ yield\ (\%) = \frac{C_{NADH}}{C_{NAD^+}} \times 100 \qquad (2)$$

Where, C_{NADH} is the concentration of regenerated NADH calculated from equation 1, C_{NAD^+} is the initial concentration of NAD^+ (1 mM) in the reaction mixture.

2.5. Detection of Reactive Oxygen Species (ROS):

2',7'-dichlorodihydrofluorescien diacetate (H_2DCFDA) was used as a general probe to detect different reactive oxygen species (ROS).[33] The presence of ROS like $O_2^{\bullet-}$, $OH^{\bullet}$ and H_2O_2 can be detected by a fluorescence signal as a result of oxidation of H_2DCFDA to 2',7'-dichlorofluroscien (DCF) (Scheme 2.1). To the irradiated reaction mixture, 5 μM H_2DCFDA was added and the mixture was kept for incubation in the dark for 1 h under stirring conditions. Photoluminescence spectra (PL) were recorded at 480 nm excitation, and enhancement in PL intensity at ~525 nm was monitored to determine the formation of ROS under our reaction conditions.

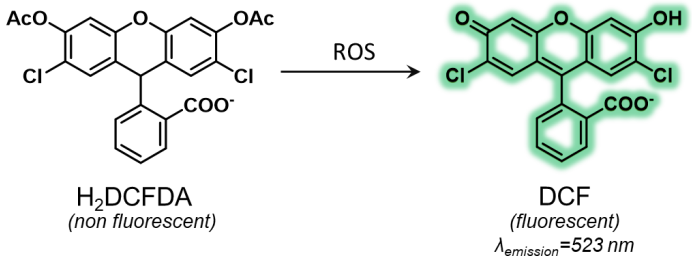

Scheme 2.1: Schematic representation for oxidation of non-fluorescent H_2DCFDA by ROS to its oxidized fluorescent form DCF.

2.5.1 Determination of Hydroxyl Radicals: Terephthalic acid was used as a probe used to detect $OH^{\bullet}$.[34] In a typical reaction, 2 mM of terephthalic acid (prepared in 2 mM NaOH) and 5 mg catalyst in 50 mM phosphate buffer (pH=7.4) were mixed and irradiated with 532 nm light for 10 h. PL spectra were recorded at 310 nm excitation post-irradiation, where enhancement in PL intensity at ~425 nm was monitored to establish the presence of OH radicals (Scheme 2.2).

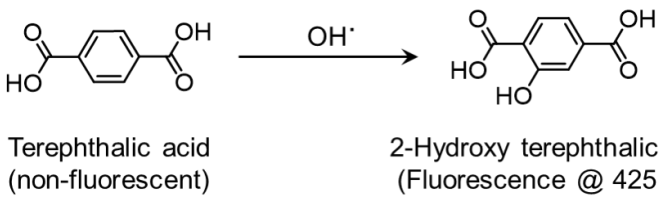

Scheme 2.2: A scheme for oxidation of non-fluorescent terephthalic acid by hydroxyl radicals to fluorescent hydroxy terephthalic acid.

2.5.2 Determination of Hydrogen Peroxide: The presence of H_2O_2 was detected using a 3,3',5,5'-tetramethylbenzidine (TMB) based colorimetric assay. In the presence of horseradish peroxidase (HRP) enzyme, H_2O_2 is reduced to O_2 while TMB is oxidized to yield a blue-colored charge transfer complex (Scheme 2.3).[35] The amount of H_2O_2 present in the reaction mixture was monitored through UV-vis absorption spectroscopy.

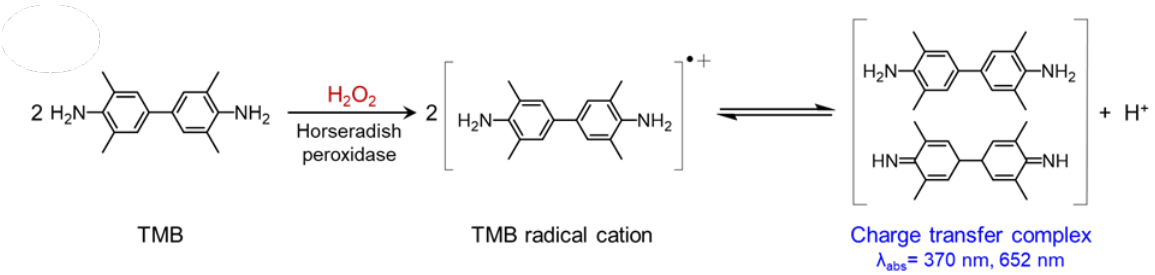

Scheme 2.3: Schematic representation for determination of hydrogen peroxide through oxidation of TMB in presence of horseradish peroxidase enzyme.

2.5.3 Determination of Superoxide Radicals: The presence of superoxide radicals ($O_2^{\bullet-}$) was estimated with nitro blue tetrazolium chloride (NBT) based assay. NBT reacts with $O_2^{\bullet-}$ to form insoluble formazan, which results in a decrease in absorbance at ~265 nm corresponding to NBT (Scheme 2.4).[34] Typically, a mixture of Au-TiO_2 and 25 µM NBT was irradiated for 10 h and was analyzed for $O_2^{\bullet-}$ through UV-vis absorption spectroscopy.

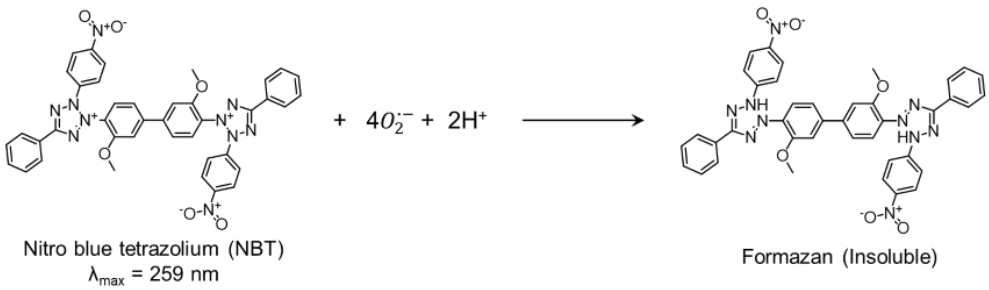

Scheme 2.4: Scheme representing determination of superoxide radical via oxidation of NBT to form formazan.

Prior literature suggests that *sole* plasmonic photocatalysis is limited by yields, manifested in ultrafast charge recombination dynamics. Integrating appropriate semiconductor into plasmonic NPs is one of the strategies to enhance the charge separation process by forming Schottky barrier at the heterojunction. With a focus on enhancing yield in plasmonic photocatalysis, we chose Au-TiO_2 plasmonic metal-semiconductor hybrid nanostructures to drive the photoregeneration of nicotinamide cofactor (NADH) under plasmonic excitation. The appropriate band alignment of Au-TiO_2 with respect to NADH regeneration allows for the directional flow of charge carriers from Au to TiO_2 upon plasmonic excitation.

3.1. Synthesis of Au-TiO_2 Hybrid Structure

The desired Au-TiO_2 hybrid nanostructures were synthesized using a deposition-precipitation method by modifying the reported in-situ borohydride reduction procedure (Figure 3.1a).[31] A range of hybrid nanostructures compositions (AT-X, X=1,2,3 etc) were obtained by adding different amount of $HAuCl_4$ to the suspension of commercially available TiO_2. A prompt color change from white to reddish-pink upon the addition of sodium borohydride was observed, suggesting the formation of AuNPs over TiO_2 (Figure 3.1 b). The intensity of plasmonic color increased with an increase in the Au content, as observed from the optical photographs in Figure 3.1b.

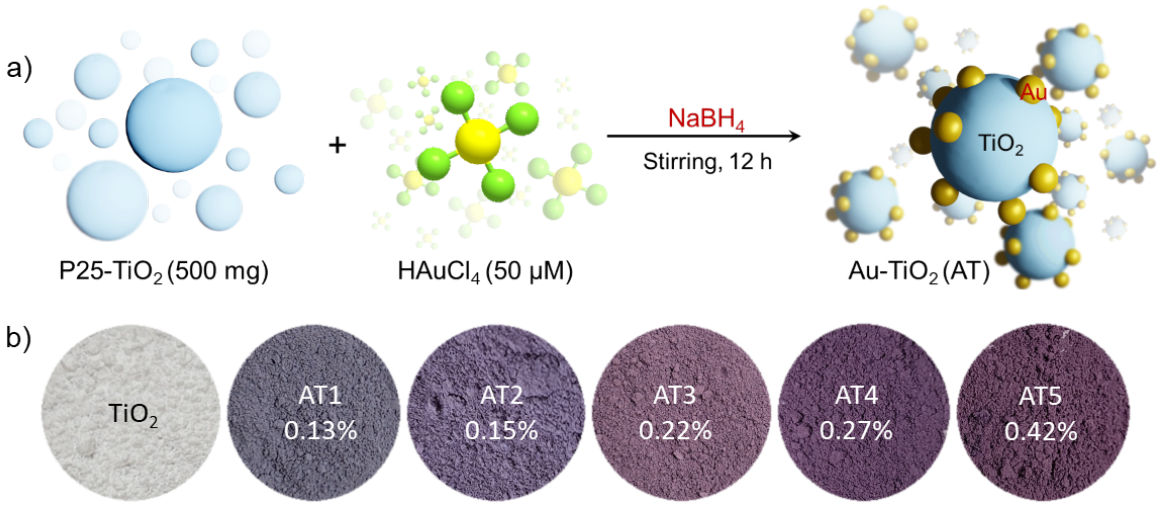

Figure 3.1: Synthesis of Au-TiO_2 hybrid photocatalyst. a) Schematic illustration of typical deposition-precipitation method for the synthesis of Au-TiO_2 photocatalyst. b) Optical photographs of Au-TiO_2 hybrid photocatalysts with different Au loading. The plasmonic colour intensifies with increase in the Au content.

UV-vis-NIR diffuse reflectance spectra clearly show the plasmonic features between 400-600 nm for different Au-TiO_2 hybrid nanostructures as opposed to only TiO_2, which predominantly absorbs in the UV region. On increasing the Au content in the hybrid catalyst, the relative intensity ratio of the LSPR band (500-600 nm) and TiO_2 band (200-300 nm) increases (Figure 3.2a). The plasmon band broadens upon increasing the Au content, and this broadening of the plasmon bands can be correlated to the inhomogeneity of the AuNPs deposited as well as the surrounding TiO_2 matrix, which is clearly observed from TEM images (Figures 3.2 b, c and Figure A1).

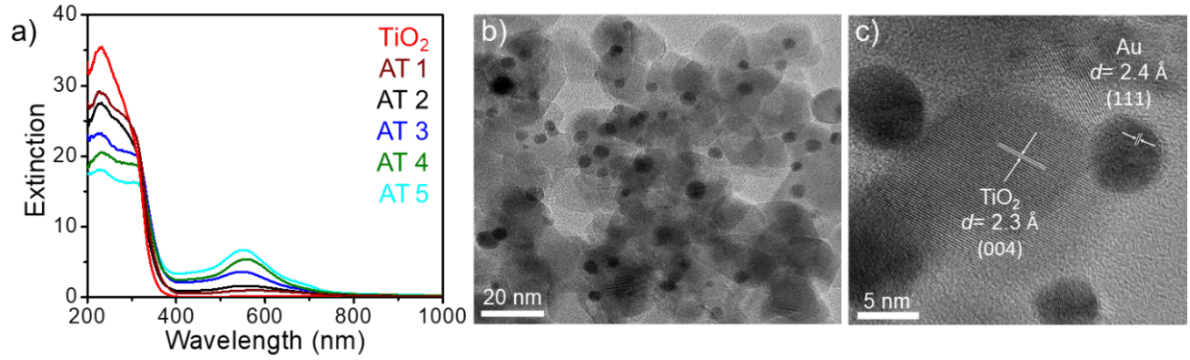

Figure 3.2: Characterization of Au-TiO_2 hybrid nanostructures a) UV-vis-NIR extinction spectrum of Au-TiO_2 photocatalysts with different Au content. b) and c) Transmission electron microscopy (TEM) images of Au-TiO_2 hybrid photocatalyst, clearly showing the deposition of AuNPs over TiO_2.

The interplanar spacing of AuNPs and TiO_2 in the hybrid heterostructure was estimated to be 0.24 nm and 0.23 nm, corresponding to (111) and (004) planes, respectively.[36,37] The exact amount of Au in different Au-TiO_2 hybrid nanostructures was calculated from ICP-MS analysis (Table 3.1). The Au content was found to be 0.13, 0.15, 0.22, 0.27, and 0.42 wt % for AT-1, AT-2, AT-3, AT-4 and AT-5 Au-TiO_2 heterostructures, respectively. After a successful synthesis and characterization, the photocatalytic activity of the Au-TiO_2 heterostructures was tested for the regeneration of nicotinamide cofactors under visible-light irradiation.

Photocatalyst	Concentration of Au (ppb)	Wt. % of Au
AT-1	1.96	0.13
AT-2	2.13	0.15
AT-3	3.21	0.22
AT-4	3.92	0.27
AT-5	6.04	0.42

Table 3.1: Au content in different hybrid structures estimated from inductively coupled plasma mass spectroscopy (ICP-MS)

3.2. Photocatalytic Regeneration of Nicotinamide Cofactor

Nicotinamide cofactors play a crucial role in enzyme-driven biocatalytic transformations and are key to devising artificial photosynthetic machinery.[17-20] As a result, there is a large interest in regenerating these cofactors under photocatalytic conditions. Moreover, the regeneration of NADH has served as a model reaction to verify several hypotheses in plasmonic photocatalysis.[21-26] *'Sole'* plasmonic photocatalysis with AuNPs has revealed the potential of plasmonic excitation in driving multielectron regeneration of NADH cofactors.[23] However, the yield of the NADH photoregeneration was low.

Here, our main idea was to enhance the efficiency of NADH regeneration in a plasmonic photocatalyzed reaction with the Au-TiO_2 metal-semiconductor hybrid system. Foremost, we checked the enhancement in the charge carrier separation by performing photocurrent measurements with different Au-TiO_2 catalysts. Au-TiO_2 hybrid was coated over FTO plate (1 x 1 cm^2 area), and photocurrent measurements were performed using a three-electrode system, with Au-TiO_2 coated FTO as the working electrode, Ag/AgCl as the reference electrode, and Pt as the counter/auxiliary electrode. A clear enhancement in the photocurrent density for Au-TiO_2 was observed as compared to only AuNPs under plasmonic excitation (Figures 3.3a and Figure A2). It can be inferred that Au-TiO_2 helps in better charge separation upon photoexcitation, when compared to only AuNPs, hence prolonging the lifetime of the charge carriers.

After establishing the enhanced charge separation in Au-TiO_2 hybrid plasmonic nanostructures, we utilized these charge carriers for the photoregeneration of the NADH cofactor. The photocatalytic regeneration of NADH was performed with Au-TiO_2 hybrid photocatalysts and TEOA as hole scavenger,irradiated with 2 x 10 W 532 nm LEDs (total light intensity measured at the test tube walls was measured to be ~230 $mWcm^{-2}$). The photoregeneration of NAD^+ to NADH was monitored using UV-vis absorption spectroscopy, where the optical density of the characteristic peak for NADH at ~340 nm was used for the yield calculation (340 nm corresponds to π- π* transitions in the nicotinamide ring).[23,32] A clear appearance of a new peak ~340 nm was observed after photoirradiation of the reaction mixture for ~10 h, confirming the successful reduction of NAD^+ to NADH (Figure 3.3b). A yield of ~30 % was estimated according to equations 1 and 2, when AT-3 was used as the photocatalyst.

Further, different reaction parameters, such as Au loading and irradiation time, were fine-tuned and optimized. A volcano-shape trend was observed while evaluating the effect of different Au content (0.13 wt. % - 0.42 wt. %) on the photocatalytic activity (Figures 3.3c). Out of different Au-TiO_2 photocatalysts, AT-3 (0.22 wt. %) gave the best conversion (Figure A3). This can be attributed to the balance between the generation of hot charge carriers, as well as the availability of adequate adsorption sites on Au and TiO_2 surfaces. This can be attributed to the appropriate balance between the generation of hot charge carriers and the availability of adequate adsorption sites on Au and TiO_2 surfaces. A lower NADH yield at lower Au content indicates a fewer heterojunction formation, therefore decreasing the overall efficiency of the reaction. Whilst an increase in Au content lowers the yield of NADH possibly due to excessive coverage by AuNPs, thereby, decreasing the sites for NAD^+ adsorption on TiO_2. Consequently, AT-3 containing 0.22 wt. % Au was chosen for further studies.

-

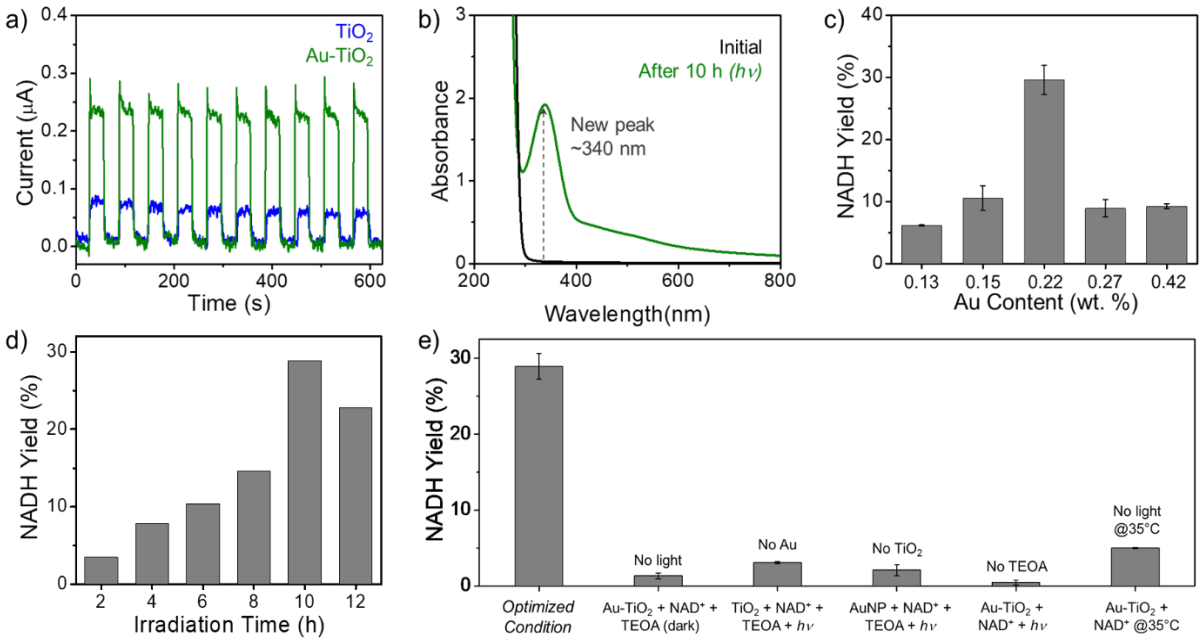

Figure 3.3. Photocatalytic regeneration of nicotinamide cofactor with Au-TiO_2 hybrid photocatalysts. a) Photocurrent measurements with Au-TiO_2 hybrid nanostructure in comparison with only AuNPs, under plasmonic excitation. b) UV-visible absorption changes in the reaction mixture before and after visible-light irradiation (532 nm) for 10 h. c) Bar diagram comparing the effect of AuNP loading on the photoregeneration of NADH cofactor by Au-TiO_2 hybrid photocatalysts. d) Bar diagram showing the time-dependent NADH formation. e) Bar diagram comparing the role of different reaction components in NADH regeneration (control reactions), proving a 12-fold enhancement in the NADH regeneration by Au-TiO_2 hybrid photocatalyst compared to sole Au catalyst.

One of the key issues with NADH regeneration is its photodegradation upon prolonged light illumination, resulting in a decrease in photocatalytic efficiency.[39] To minimize the photodegradation of the regenerated NADH, we performed a time-dependent study with AT-3 as the photocatalyst (Figure A4). With an increase in time, NADH yield also increased gradually and reached a maximum of ~30 % within 10 h of continuous light irradiation (Figures 3.3d). A further increase in the irradiation time led to a drop in the NADH yield to ~23 %, which is due to the photodegradation, as observed in prior literature reports as well.[23] Hence, all the further reactions were performed for 10 h under continuous visible-light irradiation (532 nm). Under the optimized reaction condition, a series of control experiments were performed to confirm the active role of each component in the reaction mixture (Figures 3.3e, Figure A5). Reactions performed in the absence of (i) light and (ii) TEOA (hole scavenger) gave negligible NAD+ conversion, confirming the need for both light and hole scavenger for the reaction to occur efficiently (Figure 3.3e). Control experiment in the absence of light at

elevated temperature of ~35°C gave only a marginal conversion of NADH (~5% yield), which confirms that photothermal effects have negligible role in the present study (Figure 3.3e). Next, the photocatalytic activity of individual components in a hybrid nanostructure was tested (Figure 3.3e). TiO_2 is a wide bandgap semiconductor, having a poor absorption in the visible region. As a result, a negligible amount of NADH was regenerated with only TiO_2 as the photocatalyst. On the other hand, the LSPR of AuNPs overlaps with the excitation wavelength ~532 nm. However, the photocatalytic reaction with AuNPs as the sole catalyst also resulted in a poor NADH regeneration yield. This is because of the ultrafast relaxation dynamics of the photoexcited charge carriers in AuNPs (1-100 fs), which prevent their efficient extraction for chemical conversion. It is to be noted that the total Au content in AuNP photocatalyst was normalized with respect to Au content present in AT-3.

From all these control experiments, it can be concluded that the integration of TiO_2 into the plasmonic AuNP photocatalyst led to a 12-fold enhancement in the NADH photoregeneration. This can be attributed to the efficient electron transfer from AuNP *to TiO_2 under visible-light irradiation, as supported by the energy level alignment at the metal-semiconductor heterojunction (Scheme 1.2). The Fermi energy level (E_F) of Au lies around -5.10 eV, which will rise to -2.8 eV under photon excitation with 532 nm light (or 2.33 eV).[40] Thus, under photoexcitation, the maximum potential attained by the hot electrons in AuNPs will be higher than the conduction band potential of TiO_2 centered at ~ -3.95 eV. These highly energetic electrons can easily cross the Schottky barrier (Φ_{SB} ~ 1.1 eV) at the heterojunction. More importantly, the Schottky barrier will block the reverse-electron transfer, thereby enhancing the lifetime of the photoexcited charge carriers. On the other hand, the oxidation potential of TEOA is -3.4 eV, which makes the hole extraction from AuNP core thermodynamically feasible.[25] In this way, both photoexcited electrons and holes generated in AuNPs were utilized in the regeneration of NADH cofactor by Au-TiO_2 hybrid photocatalyst. All the experiments validate that Au-TiO_2 is a true photocatalyst and the regeneration of NADH with Au-TiO_2 under visible light irradiation is purely photocatalytic.

3.3. Characterization of Photogenerated Cofactor

It is well-known that regeneration of NADH from NAD^+ can result in the formation of all the regioisomers, namely, 1,4-NADH, 1,6-NADH, 1,2-NADH, as well as the $(NAD)_2$ dimer.[37,40] Out of all, the 1,4-NADH is the only product that is enzymatically active.[23,33] Our proton NMR studies reveal that the photoregeneration of NADH by Au-TiO_2 hybrid results in a mixture of products: 1,4-NADH, 1,6-NADH, and the decay product of 1,4-NADH. In future, the Au-TiO_2 hybrid photocatalytic system could be upgraded by incorporating electron mediators for enzymatically active selective 1,4-NADH formation. The focus of the present work was to enhance the charge separation step in plasmon-powered chemical transformations, and as desired, a 12-fold enhancement in the overall NAD^+ conversion was achieved by integrating TiO_2 semiconductor into the plasmonic AuNP photocatalyst.

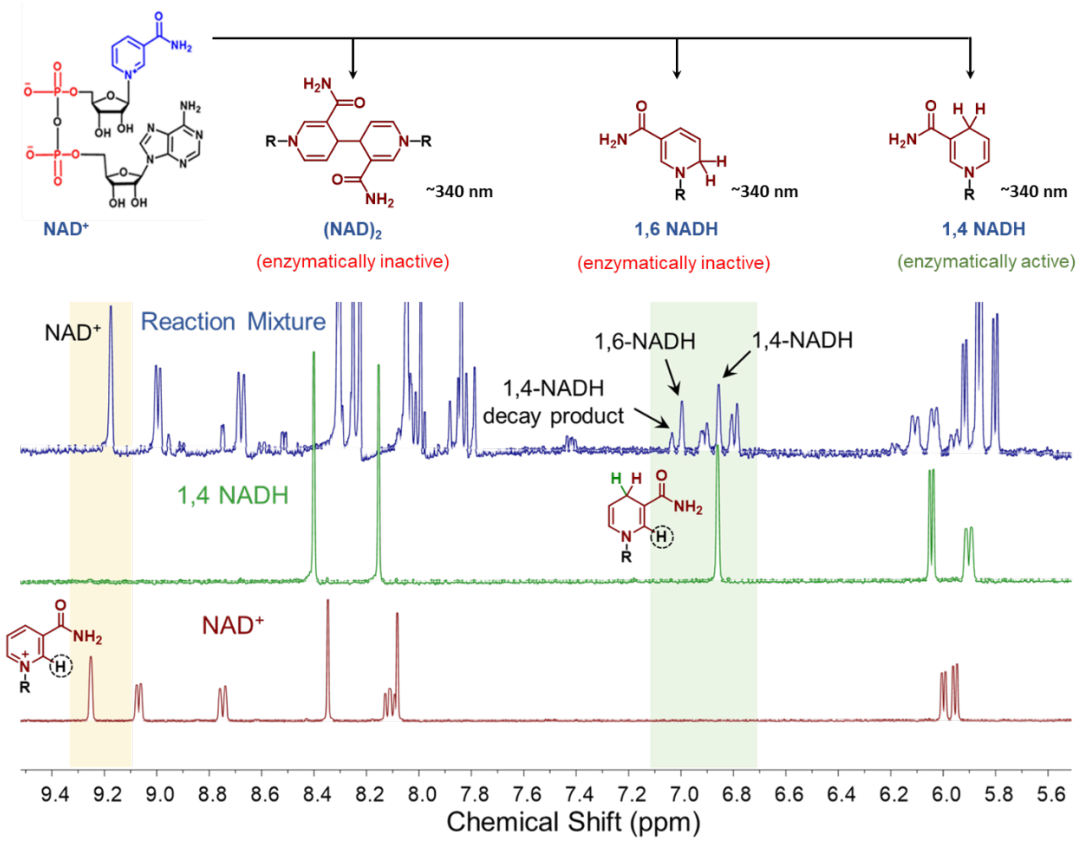

Figure 3.4. Determination of regioisomers formed upon photoreduction of NAD^+. ^{1}H-NMR spectra of pure NAD^+ (red trace), pure-1,4-NADH (green trace), and the reaction mixture containing Au-TiO_2 hybrid photocatalyst (blue trace) after 10 h of photoirradiation.

3.4. Determination of Reaction Pathway

In a previous study by Grzelczak and co-workers, NADH regeneration by conjugated microporous polymers was found to proceed in a light-independent pathway as opposed to the conventional light-dependent pathway.[41] In the light-dependent pathway, the photoexcited electrons are directly transferred to NAD^+ molecules to form NADH cofactor, while the holes are extracted by the TEOA. However, the light-independent pathway involves the capture of photoexcited electrons by oxygen molecules instead of NAD^+ molecules (Scheme 3.2), while the holes are still abstracted by the TEOA. It is the oxidized product of TEOA that converts NAD^+ to NADH in the light-independent pathway.[23] One of the oxidized products of TEOA is glycolaldehyde, which can chemically convert NAD^+ to NADH in the absence of light (Scheme 3.2).[41]

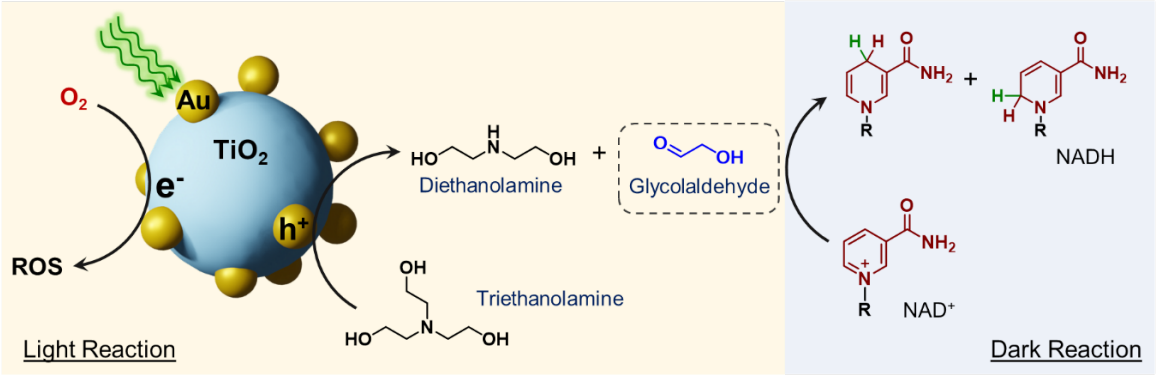

Scheme 3.1. Schematics showing the two-stage process for NADH regeneration, consisting of light-dependent and light-independent processes. Glycolaldehyde, the oxidation product from the light cycle, chemically converts NAD+ to NADH in the dark cycle.

It is known from prior literature reports that the photoregeneration of NADH by 'sole' AuNP photocatalyst follows the light-dependent pathway.[23] The strong oxygen adsorption affinity of TiO_2 could trap the oxygen molecules in the Au-TiO_2 hybrid photocatalytic system, which then could compete with NAD^+ molecules in the electron abstraction step. This motivated us to identify the pathway that was involved in the NADH photoregeneration by Au-TiO_2 hybrid photocatalytic system. A positive control experiment was carried out to verify the feasibility of chemical conversion of NAD^+ to NADH by glycolaldehyde (S6). A clear increase in the absorbance at 340 nm was observed with time, which confirms the regeneration of NADH by glycolaldehyde.

To identify the reaction mechanism in Au-TiO_2 hybrid photocatalytic system, the NADH regeneration reaction was performed in two steps: irradiating the reaction mixture containing TEOA and Au-TiO_2 hybrid photocatalyst under aerobic conditions for 10 h with visible light, and then adding the NAD^+ to this pre-irradiated reaction mixture under dark. Interestingly, we observed the appearance of a new peak at ~340 nm, and the total NADH yield reached ~40 % after 10 h incubation in the dark (Figure 3.5a). The formation as well as an increase in the NADH yield in this control experiment indicates the involvement of light-independent pathway in the photoregeneration of NADH by Au-TiO_2 hybrid photocatalytic system. The ultimate proof for the involvement of glycolaldehyde in the chemical reduction of NAD^+ to NADH was obtained by replacing TEOA with ethanol as the hole scavenger (Figure 3.5b). Control experiments with ethanol as the hole scavenger gave negligible NADH yield in light as well as dark reactions, even though the hole abstraction by ethanol was thermodynamically favorable (Figure 3.5b). The negligible product formation in ethanol can be assigned to the (i) scavenging of the photogenerated hot electrons generated in Au-TiO_2 heterostructure by O_2 molecules, thereby making them unavailable for the NAD^+ reduction, and (ii) inability of the oxidised product of ethanol (acetaldehyde) to chemically convert NAD^+ to NADH. All these control experiments prove that the identity of the hole scavenger and its oxidized product is the key to the regeneration of NADH. In short, the modification of plasmonic AuNPs with TiO_2 semiconductor not only helped in enhancing the charge separation process, but also altered the reaction mechanism.

Next, the factors influencing the chemical regeneration of NADH by glycolaldehyde in the dark cycle were studied. One such crucial factor is the pH of the solution. The reducing power of glycolaldehyde is known to increase with increase in the pH of the reaction mixture.[39,41] At pH 8, there was a slow growth of the peak at 340 nm (corresponding to NADH), with the yield reaching ~ 40 % after 10 h. Interestingly, when the pH was increased to 10.5, an acceleration in the NADH formation was observed, and the yield reached ~70 % within 10 h in the dark cycle (Figures 3.5c). It is to be noted that TEOA by itself does not reduce NAD^+ to NADH at pH 10.5 (Figure A7). Furthermore, Au-TiO_2 photocatalyst can be easily separated from the reaction mixture by centrifugation, which enabled the reuse of the photocatalyst for at least 5 cycles without any compromise in the photocatalytic activity (Figure 3.5d).

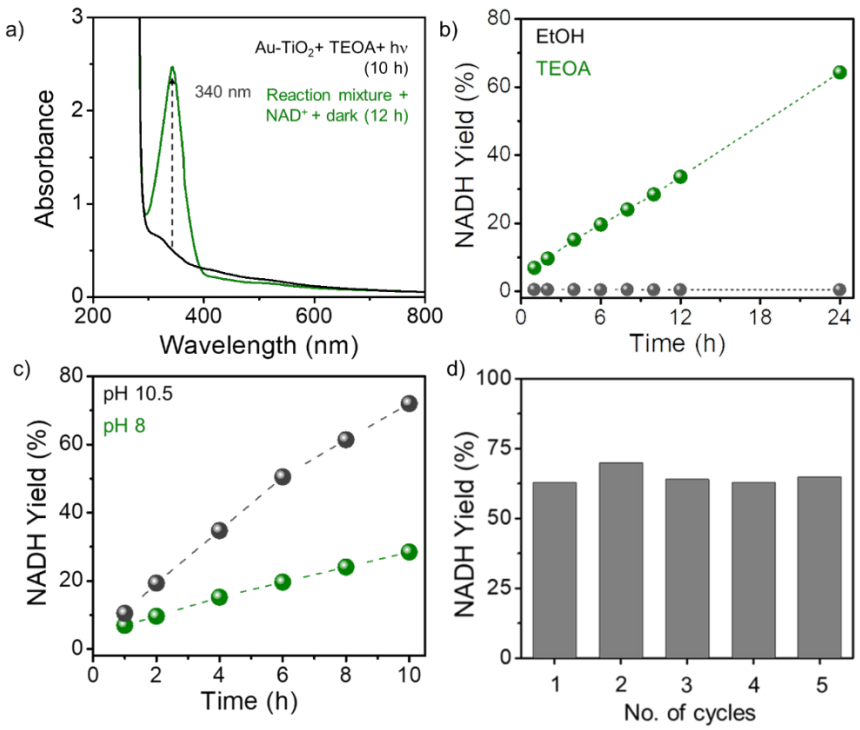

Figure 3.5. Regeneration studies to investigate the light-independent pathway. a) UV-visible absorption changes of the reaction mixture incubated in the dark, after the addition of NAD^+ to a pre-irradiated solution of Au-TiO_2 and TEOA. b) Time-dependent NADH regeneration with TEOA and ethanol as hole scavengers in the light cycle. c) Effect of pH in the chemical conversion of NAD^+ to NADH by glycolaldehyde in the light-independent (dark) cycle. d) Bar diagram showing the NADH yield with Au-TiO_2 photocatalyst for upto 5 cycles. Negligible change in the photocatalytic activity proves the excellent recyclability aspects of the photocatalyst.

3.5. Elucidating the Role of Oxygen

The active role of oxygen molecules as an electron acceptor in the present study was verified by purging the reaction mixture with argon before irradiation. The yield of the NADH formation decreased to half (~20 %) in argon, when compared to that formed under aerobic conditions (40 %) (Figure 3.6a) In general, the abstraction of the photoexcited electrons by O_2 molecules results in the formation of reactive oxygen species (ROS).[42-46] In our studies too, the presence of ROS was detected with the help of 2′,7′-dichlorodihydrofluorescein diacetate (H_2DCFDA) based assay.[33] In the presence of Au-TiO_2 photocatalyst under continuous irradiation, an enhancement of emission is seen at 525 nm, compared to that in the absence of light and photocatalyst. This confirms the presence of ROS formed as a consequence of electron transfer from Au-TiO_2 to O_2 in the photocatalytic system (Figure 3.6b). However, H_2DCFDA is a general probe of ROS and does not discriminate between different ROS. Generally,

the presence of O_2 results in the generation of hydroxyl radicals, hydrogen peroxide, and superoxide radicals. To find the identity of ROS formed under our reaction conditions, we employed specific assays for the identification of individual ROS.[33-35] The radical trapping experiments proved the generation of superoxide and hydroxyl radicals as the major ROS in the light cycle.(Figure 3.6 c,d,e) The formation of these species can be correlated to ability of TiO_2 to stabilize the reaction oxygen species (ROS) on its surface.[42-46] The identification of ROS as participating components in the reduction half reaction gave credibility to the proposed mechanism, where the cofactor reduction is proceeding via a light independent pathway.[41]

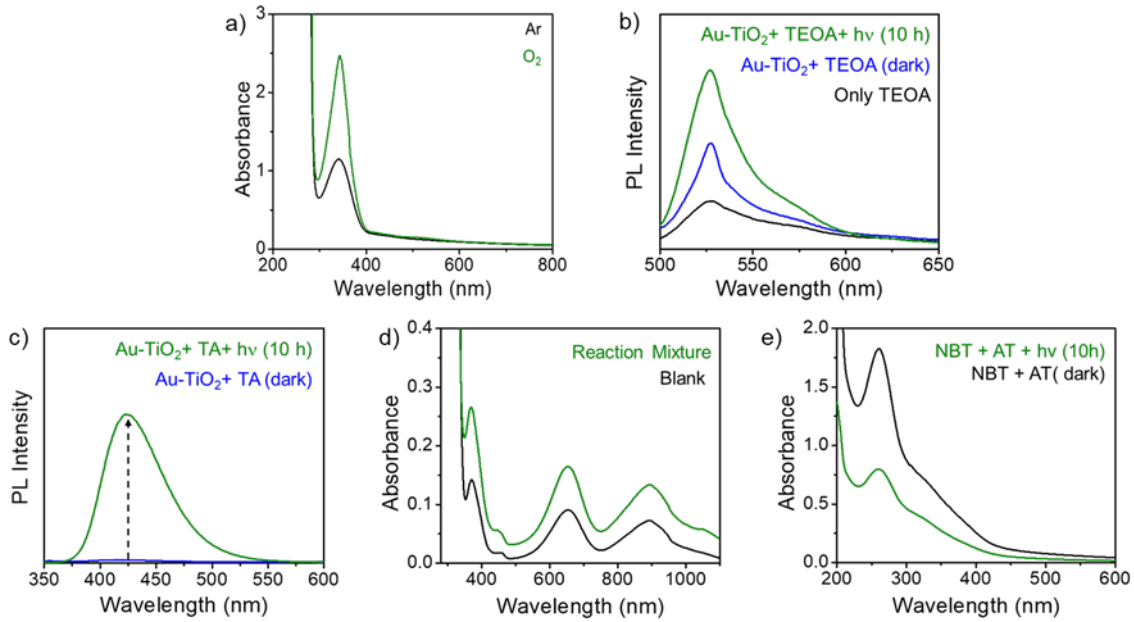

Figure 3.6. Determination of ROS species in the photoirradiated reaction mixture. a) UV-visible absorption spectra of the pre-irradiated reaction mixture (Au-TiO_2 + TEOA) after 10 h incubation in dark in presence of NAD^+, proving the critical role of molecular O_2 in abstracting the hot electrons in the light cycle. b) Emission spectra of H_2DCFDA in response to the detection of ROS species. c) Photoluminescence study with terephthalic acid for detection of hydroxyl radicals. d) UV-vis absorption changes of the reaction mixture incubated with TMB and horseradish peroxidase enzyme for determination of H_2O_2 in the photocatalytic reaction. e) UV-vis absorption changes of the reaction mixture in presence of NBT.

Doing chemistry with plasmons is exciting; however, plasmon-powered processes are intricate systems because of the involvement of various catalyst and reaction-specific parameters. Some of the major challenges associated with plasmonic photocatalysis are related to the efficient extraction of hot charge carriers and establishing the underlying mechanism. These challenges are directly or indirectly manifested in inherent plasmon relaxation dynamics. Through this study, we have overcome the

inherent limitation of inefficient charge separation in plasmonic photocatalysis by the integration of rationally chosen materials for the directional flow of charges. The charge separation process was enhanced by constructing a heterostructure between plasmonic AuNPs and n-type TiO_2 semiconductor. The formation of a Schottky barrier at the Au-TiO_2 heterojunction restricts the back-electron transfer process, which in turn enhances the lifetime of the charge-separated states. As a result, there was a 12-fold enhancement in the NADH regeneration under visible-light excitation. More importantly, the integration of TiO_2 semiconductor into plasmonic AuNPs altered the reaction mechanism involved in the regeneration of NADH cofactor as well. The stark difference in the reaction mechanism with sole AuNP and Au-TiO_2 hybrid photocatalyst also profoundly impacted the reaction yield. Furthermore, the change in reaction mechanism also alleviated the issues of product degradation under prolonged irradiation, as is commonly seen in photocatalytic NADH regeneration in literature.

Chapter 4 *Conclusions*

In summary, our study presents a strategy to enhance the plasmonic photocatalytic activity of AuNPs for the regeneration of nicotinamide cofactors under visible-light excitation. The integration of TiO_2 semiconductor into plasmonic AuNPs enhanced the charge separation process, because of the formation of a Schottky barrier at the Au-TiO_2 heterojunction. This led to a 12-fold increment in the plasmonic AuNP driven photoregeneration of NADH. Alongside, the integration of TiO_2 semiconductor into plasmonic AuNPs altered the reaction mechanism involved in the photoregeneration of NADH cofactor. Au-TiO_2 hybrid photocatalyst followed a light-independent pathway, as opposed to the light-dependent pathway followed by sole plasmonic AuNP photocatalysts. This change in the reaction mechanism helped in overcoming the problem of lower yield arising due to the prolonged photodegradation of NADH. In future, the reaction-specific studies with similar hybrid materials could enhance the overall photocatalytic conversions, as well as pave the way to unravelling the less-explored or unprecedented reaction mechanisms.

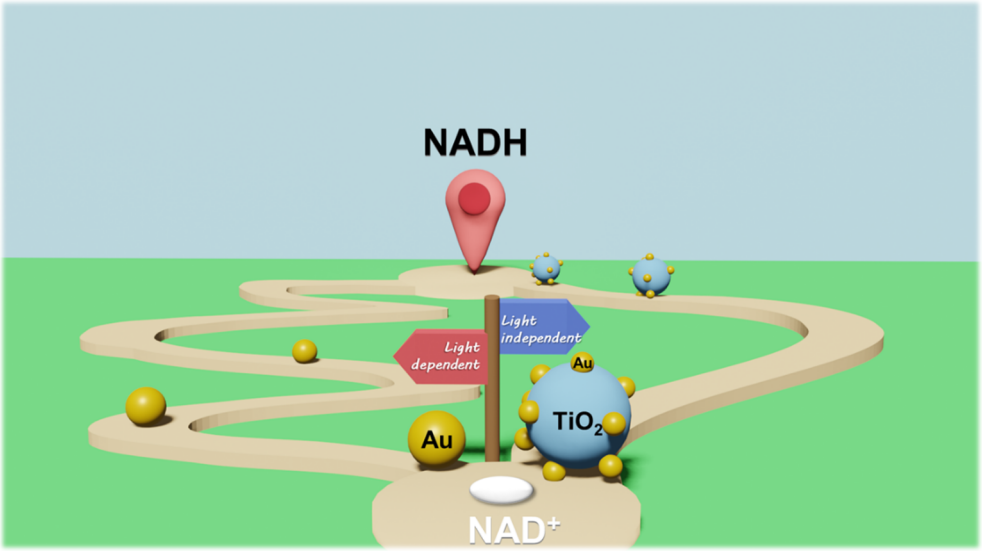

The work carried out as part of my MS thesis has been published in Photochemsitry and Photobiology journal

Namitha Deepak, Vanshika Jain, Pramod P. Pillai, Metal-semiconductor heterojunction accelerates the plasmonically powered photoregeneration of biological cofactors. *Photochem. Photobio.* **2024** **DOI:** 10.1111/php.13937

References

1. Christopher, P.; Xin, H.; Linic, S. Visible-Light-Enhanced Catalytic Oxidation Reactions on Plasmonic Silver Nanostructures. *Nat. Chem.* **2011**, *3*, 467–472.

2. Linic, S.; Christopher, P.; Ingram, D. B. Plasmonic-Metal Nanostructures for Efficient Conversion of Solar to Chemical Energy. *Nat. Mater.* **2011**, *10*, 911–921.

3. Mukherjee, S.; Libisch, F.; Large, N.; Neumann, O.; Brown, L. V.; Cheng, J.; Lassiter, J. B.; Carter, E. A.; Nordlander, P.; Halas, N. J. Hot Electrons Do the Impossible: Plasmon-Induced Dissociation of H_2 on Au. *Nano Lett.* **2013**, *13*, 240–247.

4. Roy, S.; Roy, S.; Rao, A.; Devatha, G.; Pillai, P. P. Precise Nanoparticle–Reactant Interaction Outplays Ligand Poisoning in Visible-Light Photocatalysis. *Chem. Mater.* **2018**, *30*, 8415–8419.

5. Gellé, A.; Jin, T.; De La Garza, L.; Price, G. D.; Besteiro, L. V.; Moores, A. Applications of Plasmon-Enhanced Nanocatalysis to Organic Transformations. *Chem. Rev.* **2020**, *120*, 986–1041.

6. Devasia, D.; Das, A.; Mohan, V.; Jain, P. K. Control of Chemical Reaction Pathways by Light–Matter Coupling. *Annu. Rev. Phys. Chem.* **2021**, *72*, 423–443.

7. Jain, V.; Kashyap, R. K.; Pillai, P. P. Plasmonic Photocatalysis: Activating Chemical Bonds through Light and Plasmon. *Adv. Opt. Mater.* **2022**, *10*, 2200463.

8. Link, S.; El-Sayed, M. A. Spectral Properties and Relaxation Dynamics of Surface Plasmon Electronic Oscillations in Gold and Silver Nanodots and Nanorods. *J. Phys. Chem. B* **1999**, *103*, 8410–8426

9. Hodak, J. H.; Martini, I.; Hartland, G. V. Spectroscopy and Dynamics of Nanometer-Sized Noble Metal Particles. *J. Phys. Chem. B* **1998**, *102*, 6958–6967.

10. Brongersma, M. L.; Halas, N. J.; Nordlander, P. Plasmon-Induced Hot Carrier Science and Technology. *Nat. Nanotechnol.* **2015**, *10*, 25–34.

11. Cortés, E.; Besteiro, L. V.; Alabastri, A.; Baldi, A.; Tagliabue, G.; Demetriadou, A.; Narang, P. Challenges in Plasmonic Catalysis. *ACS Nano* **2020**, *14*, 16202–16219.

12. Hammer, B.; Norskov, J. K. Why Gold Is the Noblest of All the Metals. *Nature* **1995**, *376*, 238–240.

13. Tian, Y.; Tatsuma, T. Plasmon-Induced Photoelectrochemistry at Metal Nanoparticles Supported on Nanoporous TiO_2. *Chem. Commun.* **2004**, *16*, 1810.

14. Tian, Y.; Tatsuma, T. Mechanisms and Applications of Plasmon-Induced Charge Separation at TiO_2 Films Loaded with Gold Nanoparticles. *J. Am. Chem. Soc.* **2005**, *127*, 7632–7637.

15. Linic, S.; Chavez, S.; Elias, R. Flow and Extraction of Energy and Charge Carriers in Hybrid Plasmonic Nanostructures. *Nat. Mater.* **2021**, *20*, 916–924.

16. Da Silva, A. G. M.; Rodrigues, T. S.; Wang, J.; Camargo, P. H. C. Plasmonic Catalysis with Designer Nanoparticles. *Chem. Commun.* **2022**, *58*, 2055–2074.

17. Nocera, D. G. The Artificial Leaf. *Acc. Chem. Res.* **2012**, *45*, 767–776.

18. Lee, S. H.; Kim, J. H.; Park, C. B. Coupling Photocatalysis and Redox Biocatalysis Toward Biocatalyzed Artificial Photosynthesis. *Chem. Eur.ss J.* **2013**, *19*, 4392–4406.

19. Lee, S. H.; Choi, D. S.; Kuk, S. K.; Park, C. B. Photobiocatalysis: Activating Redox Enzymes by Direct or Indirect Transfer of Photoinduced Electrons. *Angew. Chem. Int. Ed.* **2018**, *57*, 7958–7985.

20. Yang, P. Liquid Sunlight: The Evolution of Photosynthetic Biohybrids. *Nano Lett.* **2021**, *21*, 5453–5456.

21. Sánchez-Iglesias, A.; Chuvilin, A.; Grzelczak, M. Plasmon-Driven Photoregeneration of Cofactor Molecules. *Chem. Commun.* **2015**, *51*, 5330–5333.

22. Sánchez-Iglesias, A.; Barroso, J.; Solís, D. M.; Taboada, J. M.; Obelleiro, F.; Pavlov, V.; Chuvilin, A.; Grzelczak, M. Plasmonic Substrates Comprising Gold Nanostars Efficiently Regenerate Cofactor Molecules. *J. Mater. Chem. A* **2016**, *4*, 7045–7052.

23. Roy, S.; Jain, V.; Kashyap, R. K.; Rao, A.; Pillai, P. P. Electrostatically Driven Multielectron Transfer for the Photocatalytic Regeneration of Nicotinamide Cofactor. *ACS Catal.* **2020**, *10*, 5522–5528.

24. Dhankhar, A.; Jain, V.; Chakraborty, I. N.; Pillai, P. P. Enhancing the Photocatalytic Regeneration of Nicotinamide Cofactors with Surface Engineered Plasmonic Antenna-Reactor System. *J. Photochem. Photobiol., A* **2023**, *437*, 114472.

25. Jain, V.; Chakraborty, I. N.; Raj, R. B.; Pillai, P. P. Deciphering the Role of Light Excitation Attributes in Plasmonic Photocatalysis: The Case of Nicotinamide Cofactor Regeneration. *J. Phys. Chem. C* **2023**, *127*, 5153–5161.

26. Singh, S.; Kumari, S.; Ahlawat, M.; Govind Rao, V. Photocatalytic NADH Regeneration Employing Au–Pd Core–Shell Nanoparticles: Plasmonic Modulation of Underlying Reaction Kinetics. *J. Phys. Chem. C* **2022**, *126*, 15175–15183.

27. Wang, Y.; Fang, H.-B.; Zheng, Y.-Z.; Ye, R.; Tao, X.; Chen, J.-F. Controllable Assembly of Well-Defined Monodisperse Au Nanoparticles on Hierarchical ZnO Microspheres for Enhanced Visible-Light-Driven Photocatalytic and Antibacterial Activity. *Nanoscale* **2015**, *7*, 19118–19128.

28. Zheng, B. Y.; Zhao, H.; Manjavacas, A.; McClain, M.; Nordlander, P.; Halas, N. J. Distinguishing between Plasmon-Induced and Photoexcited Carriers in a Device Geometry. *Nat. Commun.* **2015**, *6*, 7797.

29. Furube, A.; Du, L.; Hara, K.; Katoh, R.; Tachiya, M. Ultrafast Plasmon-Induced Electron Transfer from Gold Nanodots into TiO_2 Nanoparticles. *J. Am. Chem. Soc.* **2007**, *129*, 14852–14853.

30. Ratchford, D. C.; Dunkelberger, A. D.; Vurgaftman, I.; Owrutsky, J. C.; Pehrsson, P. E. Quantification of Efficient Plasmonic Hot-Electron Injection in Gold Nanoparticle–TiO_2 Films. *Nano Lett.* **2017**, *17*, 6047–6055.

31. Bu, T.-A.; Hao, Y.-C.; Gao, W.-Y.; Su, X.; Chen, L.-W.; Zhang, N.; Yin, A.-X. Promoting Photocatalytic Nitrogen Fixation with Alkali Metal Cations and Plasmonic Nanocrystals. *Nanoscale* **2019**, *11*, 10072–10079.

32. Wang, X.; Saba, T.; Yiu, H. H. P.; Howe, R. F.; Anderson, J. A.; Shi, J. Cofactor NAD(P)H Regeneration Inspired by Heterogeneous Pathways. *Chem.* **2017**, *2*, 621–654.

33. Dharmaraja, A. T.; Alvala, M.; Sriram, D.; Yogeeswari, P.; Chakrapani, H. Design, Synthesis and Evaluation of Small Molecule Reactive Oxygen Species Generators as Selective Mycobacterium Tuberculosis Inhibitors. *Chem. Commun.* **2012**, *48*, 10325.

34. Jayaram, D. T.; Runa, S.; Kemp, M. L.; Payne, C. K. Nanoparticle-Induced Oxidation of Corona Proteins Initiates an Oxidative Stress Response in Cells. *Nanoscale* **2017**, *9*, 7595–7601

35. Roy, S.; Adury, V. S. S.; Rao, A.; Roy, S.; Mukherjee, A.; Pillai, P. P. Electrostatically Directed Long-Range Self-Assembly of Nucleotides with Cationic Nanoparticles to Form Multifunctional Bioplasmonic Networks. *Angew. Chem. Int. Ed.* **2022**, *61*, e202203934

36. Hara, S.; Aisu, J.; Kato, M.; Aono, T.; Sugawa, K.; Takase, K.; Otsuki, J.; Shimizu, S.; Ikake, H. One-Pot Synthesis of Monodisperse CoFe2O4@Ag Core-Shell Nanoparticles and Their Characterization. *Nanoscale Res. Lett.* **2018**, *13*, 176.

37. Ding, J.; Huang, Z.; Zhu, J.; Kou, S.; Zhang, X.; Yang, H. Low-Temperature Synthesis of High-Ordered Anatase TiO_2 Nanotube Array Films Coated with Exposed {001} Nanofacets. *Sci. Rep,* **2015**, *5*, 17773.

38. Saba, T.; Li, J.; Burnett, J. W. H.; Howe, R. F.; Kechagiopoulos, P. N.; Wang, X. NADH Regeneration: A Case Study of Pt-Catalyzed NAD^+ Reduction with H_2. *ACS Catal.* **2021**, *11*, 283–289.

39. Wang, Y.; Jin, Y.; Wang, Z.; Xiao, G.; Su, H. A Light-Dark Cascade Procedure for the Regeneration of NADH Using Graphitic Carbon Nitride Nanosheets. *ChemPhotoChem* **2022**, *6*, e202200067.

40. Kim, Y.; Smith, J. G.; Jain, P. K. Harvesting Multiple Electron–Hole Pairs Generated through Plasmonic Excitation of Au Nanoparticles. *Nat. Chem.* **2018**, *10*, 763–769.

41. Kinastowska, K.; Liu, J.; Tobin, J. M.; Rakovich, Y.; Vilela, F.; Xu, Z.; Bartkowiak, W.; Grzelczak, M. Photocatalytic Cofactor Regeneration Involving Triethanolamine Revisited: The Critical Role of Glycolaldehyde. *Appl. Catal.* **2019**, *243*, 686–692.

42. Green, J.; Carter, E.; Murphy, D. M. Interaction of Molecular Oxygen with Oxygen Vacancies on Reduced TiO_2: Site Specific Blocking by Probe Molecules. *Chem. Phys. Lett.* **2009**, *477*, 340–344. .

43. Nosaka, Y.; Nosaka, A. Y. Generation and Detection of Reactive Oxygen Species in Photocatalysis. *Chem. Rev.* **2017**, *117*, 11302–11336.

44. Parrino, F.; Livraghi, S; Giamello, E.; Ceccato, R.; Palmisano, L. Role of Hydroxyl, Superoxide, and Nitrate Radicals on the Fate of Bromide Ions in Photocatalytic TiO_2 Suspensions. *ACS Catal.* **2020**, *10*, 7922–7931.

45. Kakuma, Y.; Nosaka, A. Y.; Nosaka, Y. Difference in TiO_2 Photocatalytic Mechanism between Rutile and Anatase Studied by the Detection of Active Oxygen and Surface Species in Water. *Phys. Chem. Chem. Phys.* **2015**, *17*, 18691-18698.

46. Jayaram, D. T.; Payne, C. K. Intracellular Generation of Superoxide by TiO_2 Nanoparticles Decreases Histone Deacetylase 9 (HDAC9), an Epigenetic Modifier. *Bioconjugate Chem.* **2020**, *31*, 1354-1361.

Appendix

Characterization of commercially available TiO_2

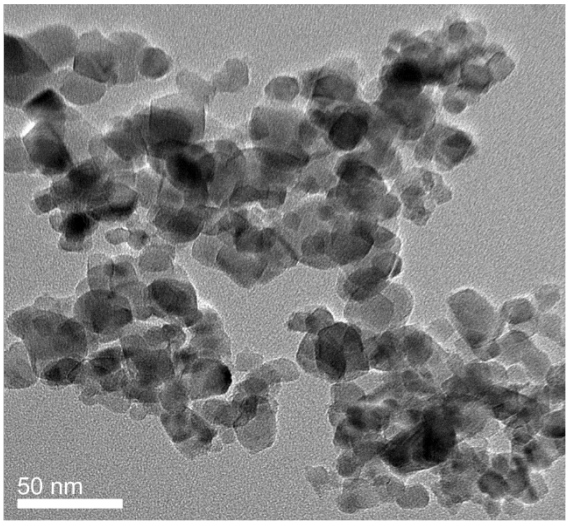

Figure A1. TEM image of TiO_2 used in the synthesis of Au-TiO_2 hybrid nanostructures. According to the values provided by Sigma-Aldrich, the particle size is ~ 21 nm. However, TEM image reveals non-uniformity in size and agglomeration, even after sonication.

Photocurrent measurements with different Au-TiO_2 photocatalysts

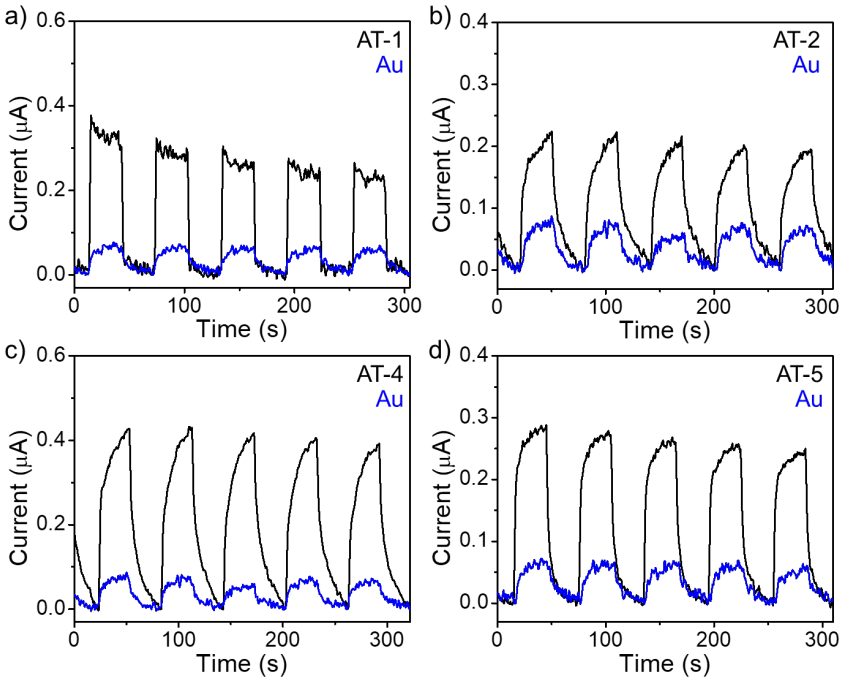

Figure A2. Photocurrent measurements of different Au-TiO_2 photocatalysts a) AT-1, b) AT-2, c) AT-4, and d) AT-5 under 532 nm irradiation. An enhancement in current is clearly observed with hybrid nanostructures as compared to only plasmonic Au NPs.

Effect of Au loading on NADH regeneration

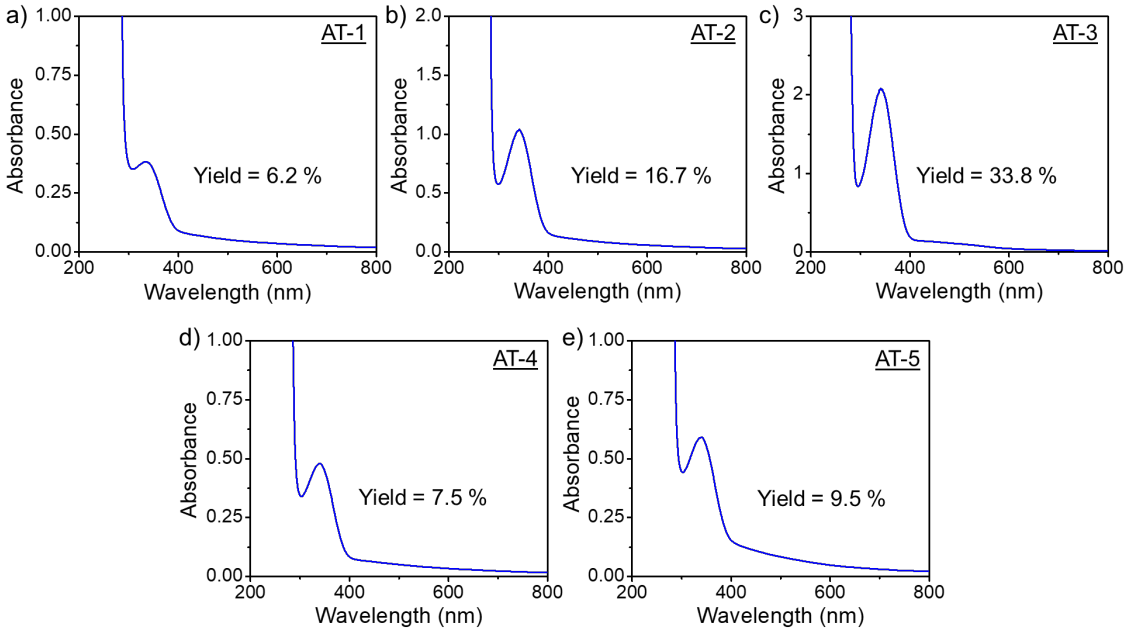

Figure A3. UV-vis absorption changes of the reaction mixture (NAD^+ + TEOA) after 10 h of visible-light irradiation with a) AT-1 (0.13 wt % Au), b) AT-2 (0.15 wt % Au), c) AT-3 (0.22 wt % Au), d) AT-4 (0.27 wt % Au), and e) AT-5 (0.42 wt % Au) as the photocatalyst.

Time-dependent NADH regeneration

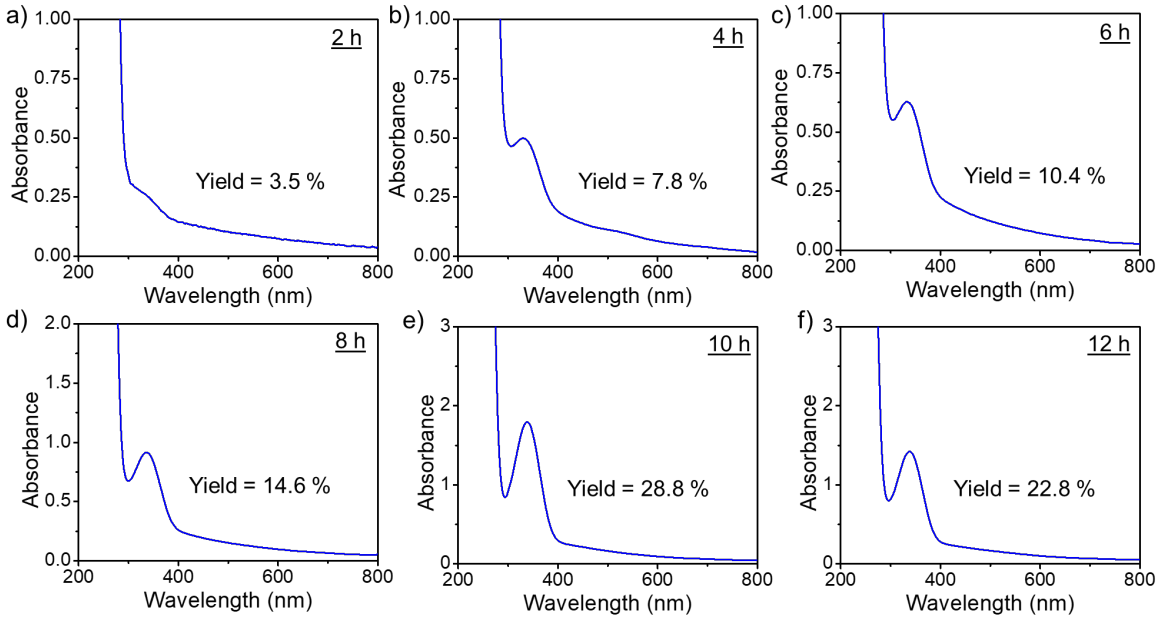

Figure A4. Effect of photoirradiation time on the yield of NADH. UV-vis absorption spectra of the reaction mixture after different irradiation time of a) 2 h, b) 4h, c) 6 h, d) 8 h, e) 10 h, and f) 12 h. Reaction conditions: 1 mM NAD^+ + 1 M TEOA + 5 mg Au-TiO_2 (0.22 wt % Au) + 50 mM PBS buffer + light (532 nm).

Photocatalytic NADH regeneration under different conditions (Control experiments)

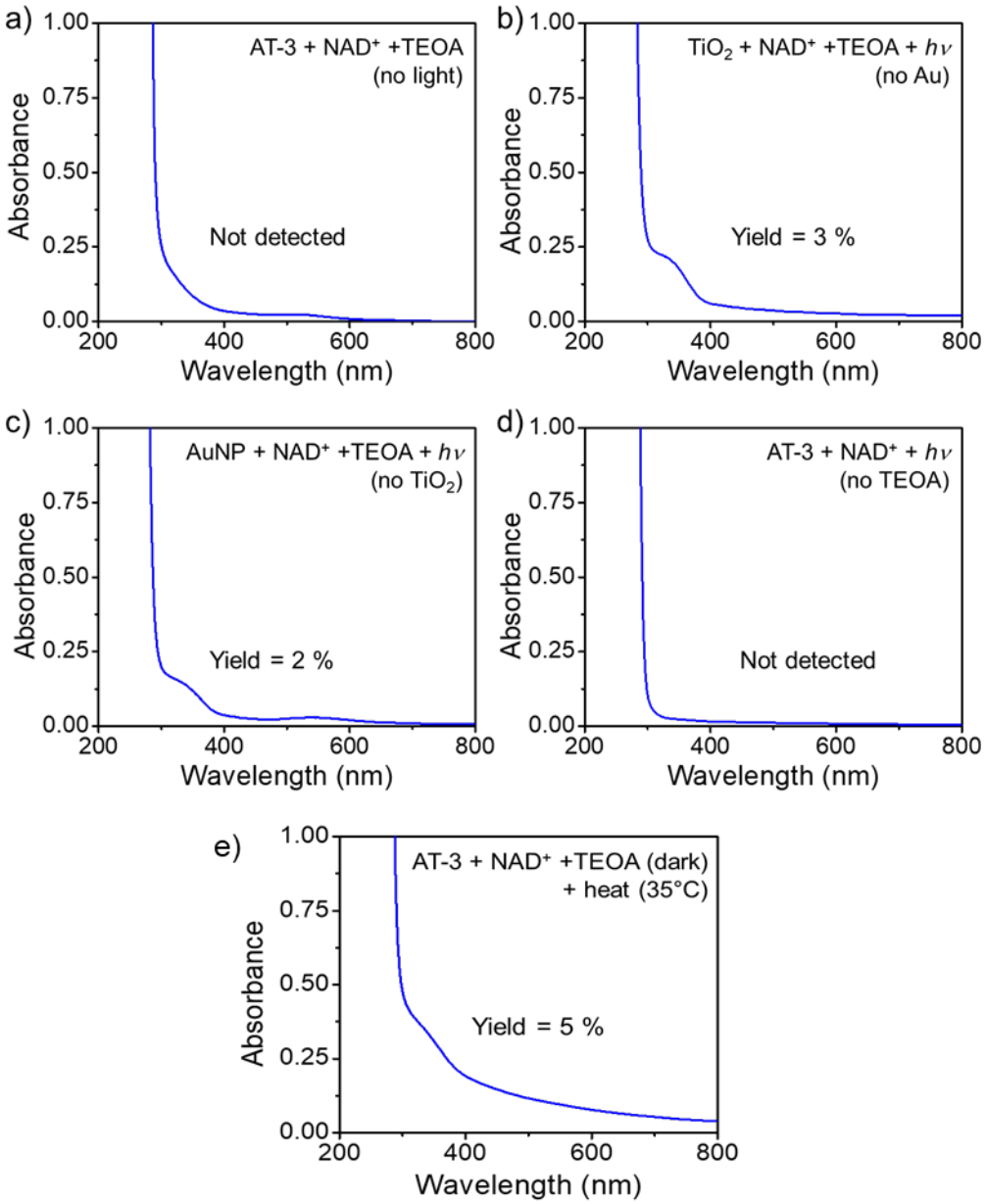

Figure A5. UV-vis absorption spectra of the reaction mixture for different control experiments performed in the absence of a) light, b) AuNP, c) TiO_2, and d) TEOA (hole scavenger).e) light @35°C The time of reaction was maintained at ~10 h in all cases.

Regeneration of NADH with glycolaldehyde in the reaction mixture (Control experiment)

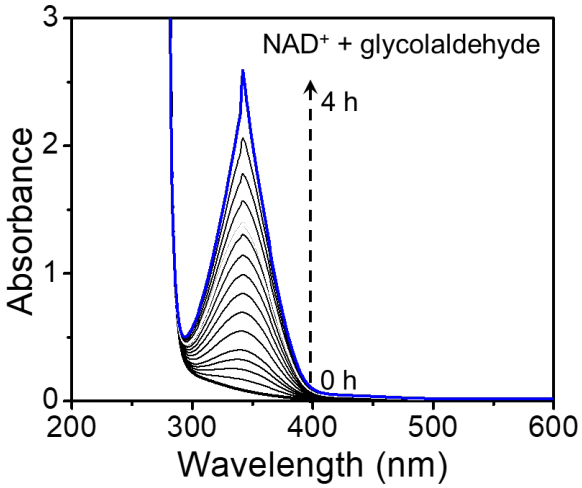

Figure A6. UV-vis absorption changes in the reaction mixture containing 1 mM NAD^+ and 1 mM glycolaldehyde in the presence of 1 M TEOA and phosphate buffer. This control experiment proves that glycolaldehyde can chemically convert NAD^+ to NADH.

Regeneration of NADH with TEOA at pH 10.5 (Control Experiment)

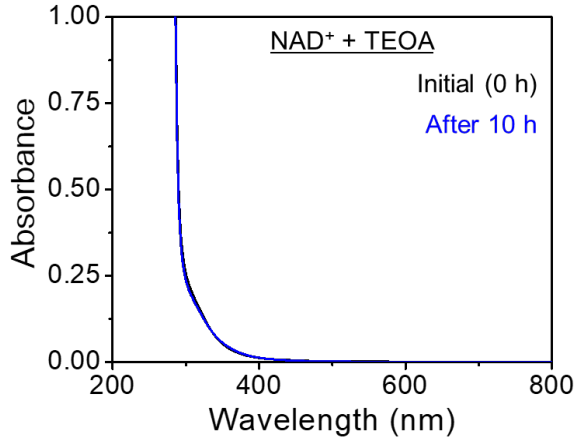

Figure A7. UV-vis absorption changes for control experiment to evaluate the reducing ability of TEOA to regenerate NADH at pH 10.5. Negligible changes in the absorption spectra proves that TEOA by itself cannot regenerate NADH at pH 10 in the absence of light.